GENERAL ATOMIC

GA-A14325

COMPARISON STUDY ON GCFR CORE SUPPORT GRID PLATE DISPLACEMENT AMONG EXPERIMENTAL, ANALYTICAL, AND FINITE-ELEMENT MODELS

by

A. S. Chuang, K. H. Chang, and C. E. Washington

This is a preprint of a paper to be presented at the Fourth International Conference on Structural Mechanics in Reactor Technology, August 15-19, 1977, San Francisco, California, and to be printed in the Proceedings.

Prepared under
Contract EY-76-C-03-0167
Project Agreement No. 23
for the
San Francisco Operations Office
U.S. Energy Research and Development Administration

General Atomic Project 3228

Date Published: March 1977

---

1. INTRODUCTION

The core support grid plate for the gas-cooled fast breeder reactor (GCFR) is a thick perforated plate into which the fuel assemblies are inserted and locked. The grid plate should be designed to be sufficiently rigid to minimize bending due to all expected service loadings which might splay the fuel assemblies apart, thus causing a reactivity change, albeit negative. In the present analysis, the equivalent solid material concept was used, and the equivalent solid plate [1-3] was treated using a transversely isotropic elasticity theory [4]. The general solution was derived for a simply supported plate subjected to a uniform load and included the solid outer rim effect.

For the finite-element model, a two-dimensional axisymmetric solid element was used. The orthotropic material behavior at the perforated region was retained, and the solid rim was modeled using isotropic material properties. The effective elastic constants for the analytical and finite-element model were determined from Refs. 5 and 6. The scaled test model was made of aluminum alloy and had a diameter of 508 mm (20 in.) and a thickness of 91.44 mm (3.6 in.). The perforated pattern consisted of penetrations having a pitch of 26.16 mm (1.03 in.) and a hole diameter of 24.2 mm (0.953 in.). The axial displacement of the grid plate model was measured at 68.95-kPa (10-psi) intervals during pressurization to a maximum pressure of 413.68 kPa (60 psi). The partial clamping effect at the edge due to the support rings was analytically treated and included in the test results for comparison.

2. THEORY AND DISPLACEMENT ANALYSIS OF GRID PLATE

2.1. MATHEMATIC FORMULATION

A thick perforated plate was treated as a transversely isotropic solid disk; the stress and strain relationships can be written as

$$\left.\begin{aligned}
\varepsilon_r &= \frac{1}{E^*}\sigma_r - \frac{\nu^*}{E^*}\sigma_\theta - \frac{\nu'}{E'}\sigma_z \quad , \quad \gamma_{rz} = \frac{1}{G'}\tau_{rz} \quad , \\
\varepsilon_\theta &= -\frac{\nu^*}{E^*}\sigma_r + \frac{1}{E^*}\sigma_\theta - \frac{\nu'}{E'}\sigma_z \quad , \quad \gamma_{\theta z} = \frac{1}{G'}\tau_{\theta z} = 0 \quad , \\
\varepsilon_z &= -\frac{\nu'}{E'}\sigma_r - \frac{\nu'}{E'}\sigma_\theta + \frac{1}{E'}\sigma_z \quad , \quad \gamma_{r\theta} = \frac{1}{G^*}\tau_{r\theta} = 0 \quad .
\end{aligned}\right\} \tag{1}$$

Using these equations, the stresses of a simply supported plate subject to a uniformly distributed load (refer to Fig. 1, except R is replaced by R_1 in Fig. 1) can be expressed as follows:

$$\sigma_r = \frac{3p}{4h^3}(3 + \nu^*)(R^2 - r^2)z + pm\left[\left(\frac{z}{h}\right)^3 - \frac{3}{20}\left(\frac{z}{h}\right)\right] \quad , \tag{2}$$

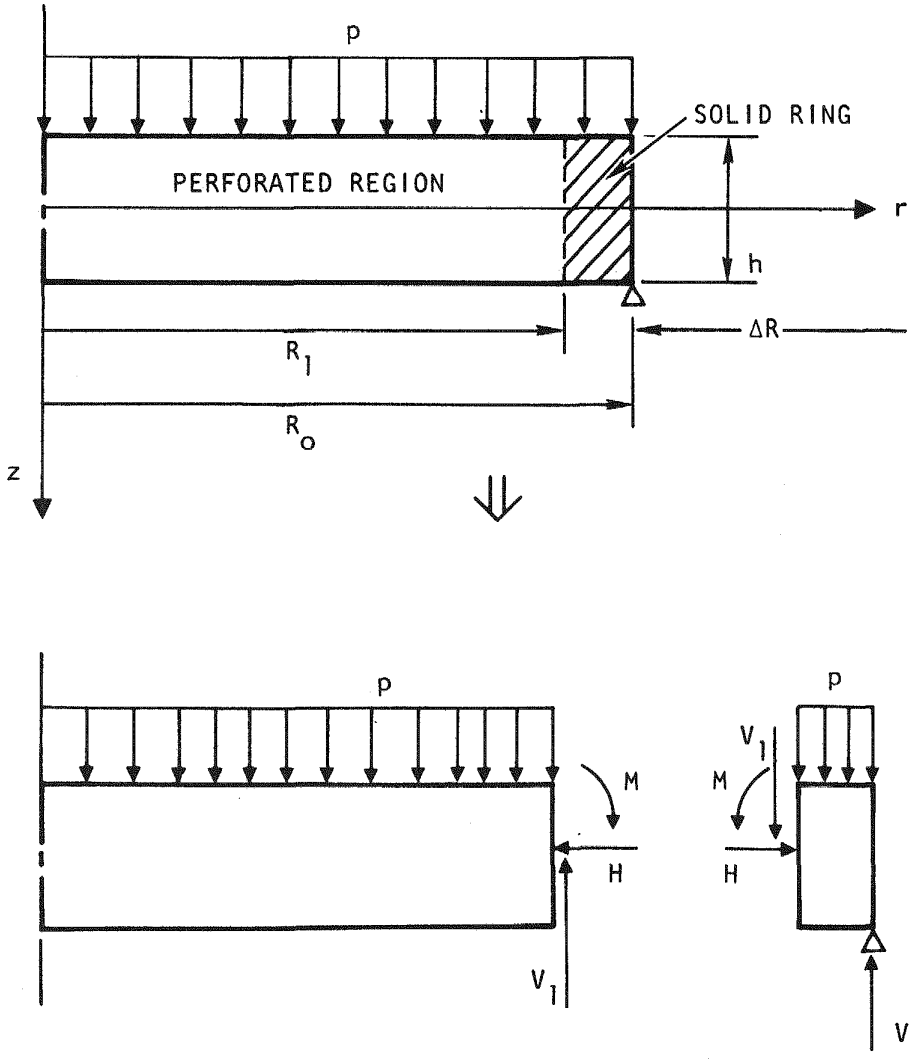

Fig. 1. Free-body diagram of the grid plate model and the solid ring

$$\left.\begin{aligned} \sigma_\theta &= \frac{3p}{4h^3}\left[(3+\nu^*)R^2 - (1+3\nu^*)r^2\right] z + pm\left[\left(\frac{z}{h}\right)^3 - \frac{3}{20}\left(\frac{z}{h}\right)\right] \quad , \\ \sigma_z &= \frac{p}{2}\left[-1 + 3\left(\frac{z}{h}\right) - 4\left(\frac{z}{h}\right)^3\right] \quad , \quad \tau_{rz} = -\frac{3p}{4h} r\left[1 - 4\left(\frac{z}{h}\right)^2\right] \quad , \end{aligned}\right\} \tag{2}$$

where $$m = \frac{E^*}{1-\nu^*}\left[\frac{1}{G'} - \frac{\nu'(3+\nu^*)}{E'}\right] \quad ,$$

E', ν', G' = Young's modulus, Poisson's ratio, and shear modulus, respectively, in the plane perpendicular to the plane of isotropy for transversely isotropic material,

E^*, ν^*, G^* = effective Young's modulus, Poisson's ratio, and shear modulus, respectively, for equivalent solid plate in the plane of isotropy for transversely isotropic material.

Using eqs. (1) and (2) and the compatibility relations, and after a lengthy derivation, the final expression of the radial and axial displacement of the grid plate can be written as

$$u_r = \frac{pr}{E^*}\left\{\frac{E^*\nu'}{2E'} + \frac{3(1-\nu^*)}{4h^3}\left[(3+\nu^*)R^2 - (1+\nu^*)r^2\right]z - \frac{3z}{20h}\left[m(1-\nu^*) + 10\frac{E^*}{E'}\nu'\right] + \frac{z^3}{h^3}\left[m(1-\nu^*) - 2\frac{E^*}{E'}\nu'\right]\right\} \quad , \tag{3}$$

$$w = \frac{p}{64D}(R^2 - r^2)\left[\frac{5+\nu^*}{1+\nu^*}R^2 - r^2\right] + \frac{3p}{10h}\left[\frac{1}{G'} - \frac{\nu'(7-\nu^*)}{4E'}\right](R^2 - r^2) + \frac{zp}{E'}\left\{-\frac{1}{2} - \frac{3\nu' z}{4E'h^3}\left[(3+\nu^*)R^2 - 2(1+\nu^*)r^2\right] + \frac{3z}{20h}\left[m\nu' + 5\right] - \frac{z^3}{2h^3}\left[m\nu' + 1\right]\right\} \quad , \tag{4}$$

where $$D = \frac{E^* h^3}{12(1-\nu^{*2})} \quad .$$

For an isotropic material, $E = E' = E^*$, $\nu = \nu' = \nu^*$, $G = G' = G^* = \frac{E}{2(1+\nu)}$, and

$$m = \frac{E^*}{1-\nu^*}\left[\frac{1}{G'} - \frac{\nu'(3+\nu^*)}{E'}\right] = 2 + \nu \quad .$$

Substituting these relations into eqs. (3) and (4), the radial and axial displacements can be reduced to

$$u_r = \frac{pr}{E}\left\{\frac{\nu}{2} + \frac{3(1-\nu)}{4h^3}\left[(3+\nu)R^2 - (1+\nu)r^2\right]z - \frac{3z}{20h}(2 + 9\nu - \nu^2) + \frac{z^3}{h^3}(2 + \nu - \nu^2)\right\} \quad , \tag{5}$$

$$w = \frac{p}{64D}(R^2 - r^2)\left[\frac{5 + \nu}{1 + \nu} R^2 - r^2\right] + \frac{3p(8 + \nu + \nu^2)}{40Eh}(R^2 - r^2)$$

$$+ \frac{pz}{E}\left\{-\frac{1}{2} - \frac{3\nu z}{4Eh^3}[(3 + \nu)R^2 - 2(1 + \nu)r^2] + \frac{3z}{20h}(5 + 2\nu + \nu^2) - \frac{z^3}{2h^3}(1 + \nu)^2\right\} \quad (6)$$

The expressions in eqs. (5) and (6) are identical to those given by Love's mathematical theory of elasticity [7].

2.2. SOLID RING EFFECT

The derivation of the transversely isotropic plates subjected to a uniformly distributed pressure is shown in Section 2.1. However, the grid plate has an outer solid ring, and the effect of this solid ring is twofold: (1) subtractive displacement caused by the discontinuous moment M and (2) additional displacement caused by the discontinuous membrane force H and the edge rotation of the grid plate. The free body diagram of the grid plate and the solid ring is shown in Fig. 1. Considering the effects of M and H, the total axial displacement of the grid plate yields

$$w_{total} = w - \frac{6}{h^3}\left[\frac{(1 - \nu^*)}{E^*}(R_1^2 - r^2) - \frac{2\nu'}{E^*}z^2\right]M + \frac{2\nu'}{E'}\frac{z}{h}H + \frac{pR_2(R_1^2 + R_0^2)\Delta R^2}{4EI} \quad . \quad (7)$$

The discontinuous moment M and membrane force H have been derived in Ref. 8 as

$$M = \frac{\dfrac{pR_1^3}{8D(1 + \nu^*)} - \dfrac{pR_2(R_1^2 + R_0^2)\Delta R}{4EI} + \dfrac{3pR_1}{5h}\left[\dfrac{1}{G'} - \dfrac{\nu_z^*(7 - \nu^*)}{E'}\right]}{\dfrac{R_1R_2}{EI} + \dfrac{12R_1(1 - \nu^*)}{E^*h^3}} \quad ,$$

$$H = \frac{pEE^*\nu'h\Delta R}{2E'[E^*R_2 + (1 - \nu^*)E\Delta R]} \quad ,$$

where $I = \dfrac{\Delta Rh^3}{12}$.

2.3. COMPUTATIONAL MODELS

2.3.1. Finite-Element Model

2.3.1.1. Application. The finite-element analysis for the grid plate was accomplished using the SAP IV computer program [9]. A two-dimensional axisymmetric solid element symmetrical to the vertical axis was employed. The equivalent solid circular plate has a 228.6-mm (9-in.) radius and a 91.44-mm (3.6-in.) thickness. There are 79 nodes in half of the symmetric model. The edge, a 25.4-mm (1-in.) wide solid ring, is modeled into 18 nodes (Fig. 2).

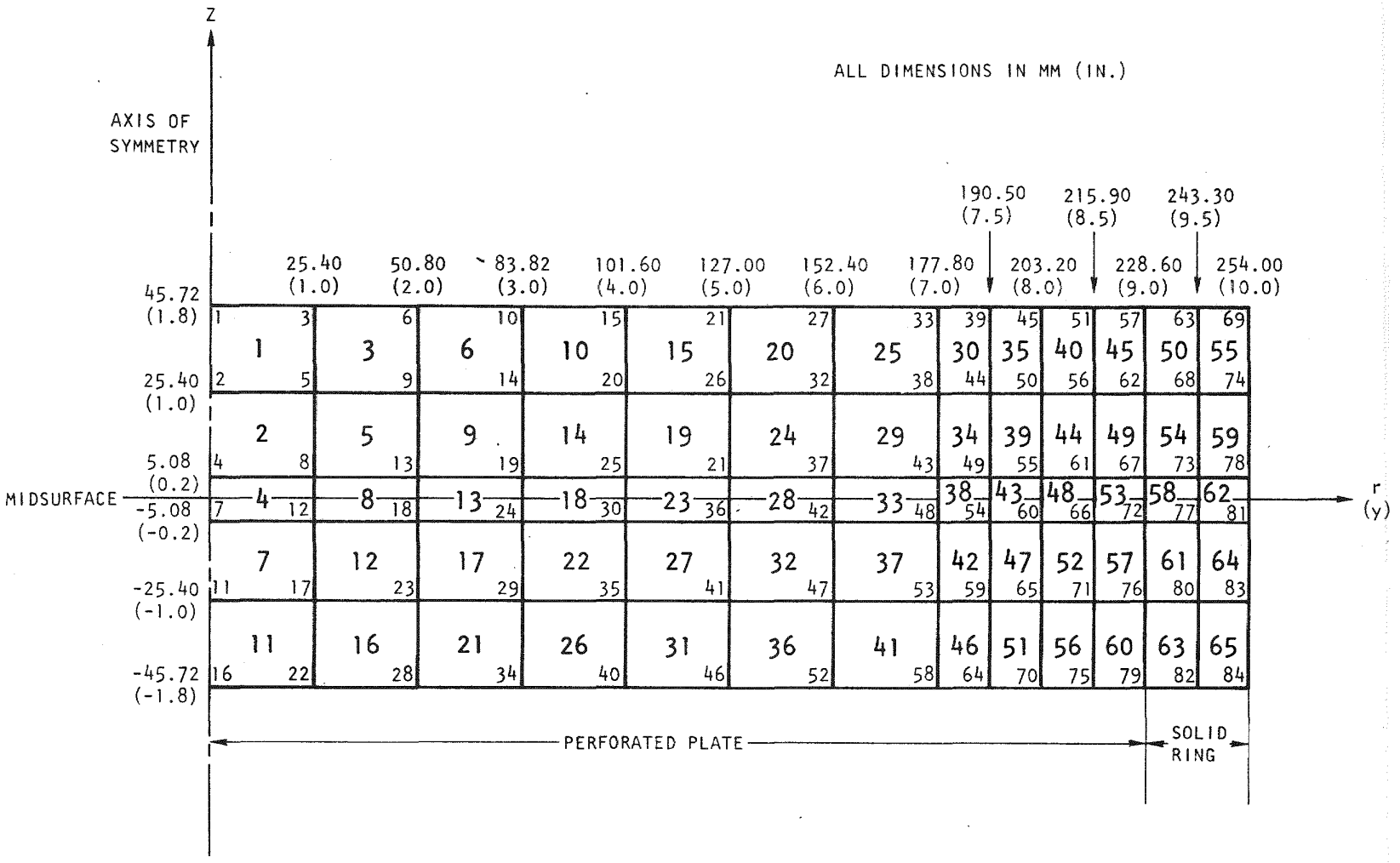

Fig. 2. Nodal arrangement of grid plate model, finite-element scheme

Based on Ref. 5, the in-plane effective elastic constants for an aluminum alloy can be determined as

$$E^* = 1.379 \times 10^3 \text{ MPa } (0.2 \times 10^6 \text{ psi}) \quad ,$$
$$\nu^* = 0.76 \quad .$$

The effective elastic constants in the axial direction can be evaluated according to Ref. 6:

$$E' = 15.561 \times 10^3 \text{ MPa } (2.257 \times 10^6 \text{ psi}) \quad ,$$
$$G' = 3.105 \times 10^3 \text{ MPa } (0.4503 \times 10^6 \text{ psi}) \quad .$$

The SAP IV input material properties are $E_r = E_\theta = E^* = 1.379 \times 10^3$ MPa (0.2×10^6 psi); $E_z = E_z^* = 15.561 \times 10^3$ MPa (2.257×10^6 psi); $G_{zr} = G_{zr}^* = 3.105 \times 10^3$ MPa (0.4503×10^6 psi); $\nu_{zr} = \nu_{z\theta} = 0.3$; $\nu_{r\theta} = \nu^* = 0.76$.

2.3.1.2. Boundary Conditions. For the finite-element model, at 9.525 mm (3/8 in.) from the outer edge of the solid ring, the grid plate is simply supported around the circumference, and the boundary conditions of the grid plate are

at $r = 0$: $u_r = 0$, $\tau_{rz} = 0$;
at $r = 244.475$ mm (9.625 in.): $u_z = 0$, $\sigma_r = 0$;
at $z = 45.720$ mm (1.8 in.): $\sigma_z = -p$;
at $z = -45.720$ mm (-1.8 in.): $\sigma_z = 0$, $\tau_{rz} = 0$.

2.3.1.3. Results. The results of finite-element analysis are shown in Fig. 3. The axial deflections of the grid plate subjected to pressures of 68.95 kPa (10 psi), 137.90 kPa (20 psi), 206.84 kPa (30 psi), 275.79 kPa (40 psi), 344.74 kPa (50 psi), and 413.68 kPa (60 psi) were plotted against the radial distance from the center of the plate. The 9.525-mm (3/8-in.) thick edge of the grid plate was clamped, and therefore, there was no deflection at this point. The maximum axial deflection at the center of the grid plate subjected to a pressure of 413.68 kPa (60 psi) was 0.2337 mm (9.2×10^{-3} in.).

2.3.2. Numerical Results of Analytical Model

Since the total axial displacement at the center of the grid plate plus the solid ring effect under a uniform pressure loading p has been formulated in terms of the geometric and material parameters in eq. (7), it can be numerically calculated, providing the physical dimension, configuration, and material are known. The material elastic constants are calculated for aluminum alloy 7075-T651 as $E = 68.947 \times 10^3$ MPa (10^7 psi); $\nu = 0.3$; $E^* = 1.379 \times 10^3$ MPa (0.2×10^6 psi); $\nu^* = 0.76$; $E' = 15.561 \times 10^3$ MPa (2.257×10^6 psi); $G' = 3.105 \times 10^3$ MPa (0.4503×10^6 psi); $\nu' = \nu = 0.3$.

The geometric dimensions of the grid plate are $R_0 = 254.0$ mm (10 in.); $R_1 = 228.6$ mm (9 in.); $R_2 = 241.30$ mm (9.5 in.); $h = 91.44$ mm (3.6 in.); $\Delta R = R_0 - R_1 = 25.4$ mm (1.0 in.).

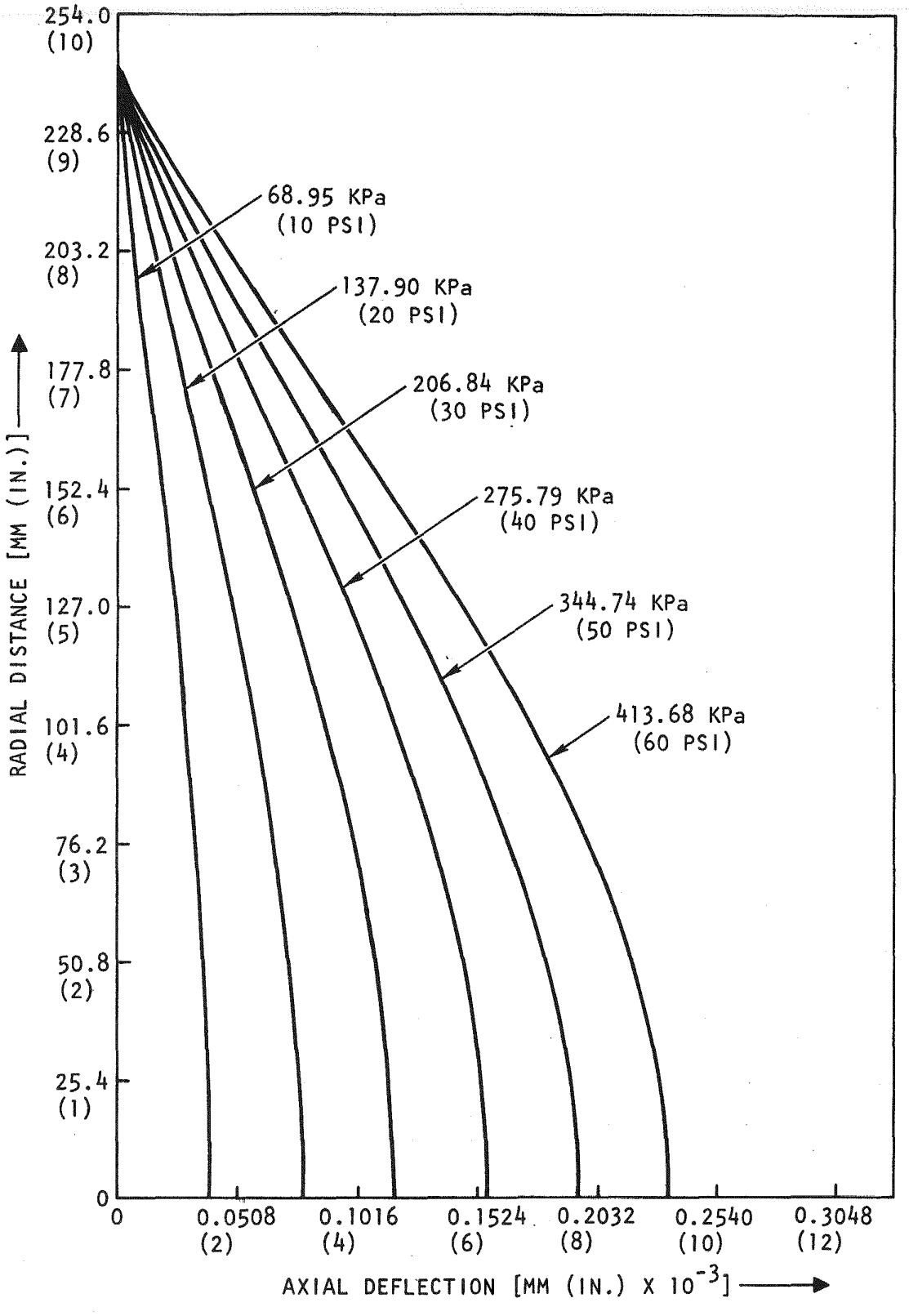

Fig. 3. Axial displacement of grid plate model by finite-element method

Based on the given elastic properties and geometric dimensions, the deflection at the center of the grid plate for a pressure loading of 413.68 kPa (60 psi), the discontinuous moment M, the discontinuous membrane force H, and the axial displacement are M = 1.0772 MN.m/m (242.17 in.-lb/in.); H = 1.1693 kN/m (6.67 lb/in.); w = 0.2384 mm (9.387×10^3 in.).

3. EXPERIMENTAL ANALYSIS OF GRID PLATE

3.1. TEST MODEL

The grid plate test model is shown in Fig. 4. The material used for the model is 7075-T651 aluminum alloy. The perforated plate consists of a triangular penetration pattern arranged in the form of a hexagonal assembly. There are 256 holes with a diameter of 24.2 mm (0.953 in.); the inner 118 holes are for the fuel assemblies, and the other 147 peripheral holes are for the blanket assemblies. The overall diameter of the grid plate model is 508 mm (20.0 in.), and it is 91.4 mm (3.6 in.) thick. The dimensions for the perforation and the boundary dividing the fuel and blanket assemblies are shown in Fig. 4.

3.2. TESTING

The axial displacement test measuring point locations are shown in Fig. 4, and the test setup and the measuring device are shown in Fig. 5. Measurements were taken with dial indicators attached to the head of the 1.3345×10^6 N (300,000 lb) testing machine (see Fig. 5). Each test consisted of setting the dial indicator gauges at zero and taking readings at 68.95-kPa (10-psi) intervals during pressurization to a maximum of 413.68 kPa (60 psi). The axial displacement versus the radial distance of the grid plate under various pressure loadings is shown in Fig. 6.

4. EFFECT OF CLAMPING ON THE EDGE OF THE GRID PLATE TEST MODEL

4.1. INTRODUCTION

Because the test model of the grid plate was clamped between two steel rings through eight preloaded bolts against the applied pressure loading, the boundary condition of the grid plate was not a simply supported case, and it was necessary to determine the effect of clamping to compare the results of the testing with numerical and analytical methods. The test setup is shown schematically in Fig. 7.

4.2. DERIVATION

The free-body diagram of the grid plate and the support rings is shown in Fig. 8. In this figure, V and Q are the edge forces exerted at the corner edges of the support ring

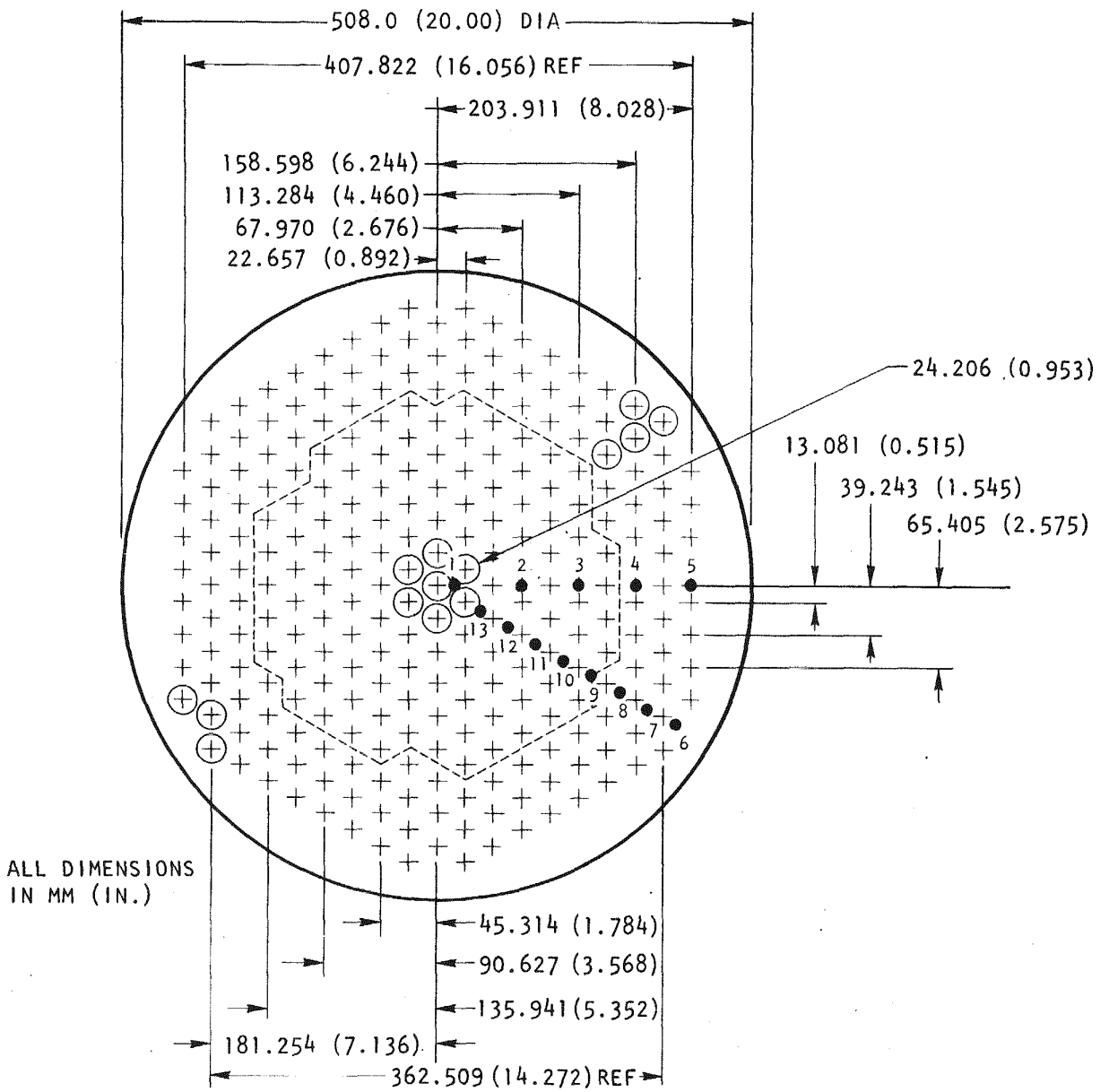

Fig. 4. Grid plate test model and axial deflection measuring point locations

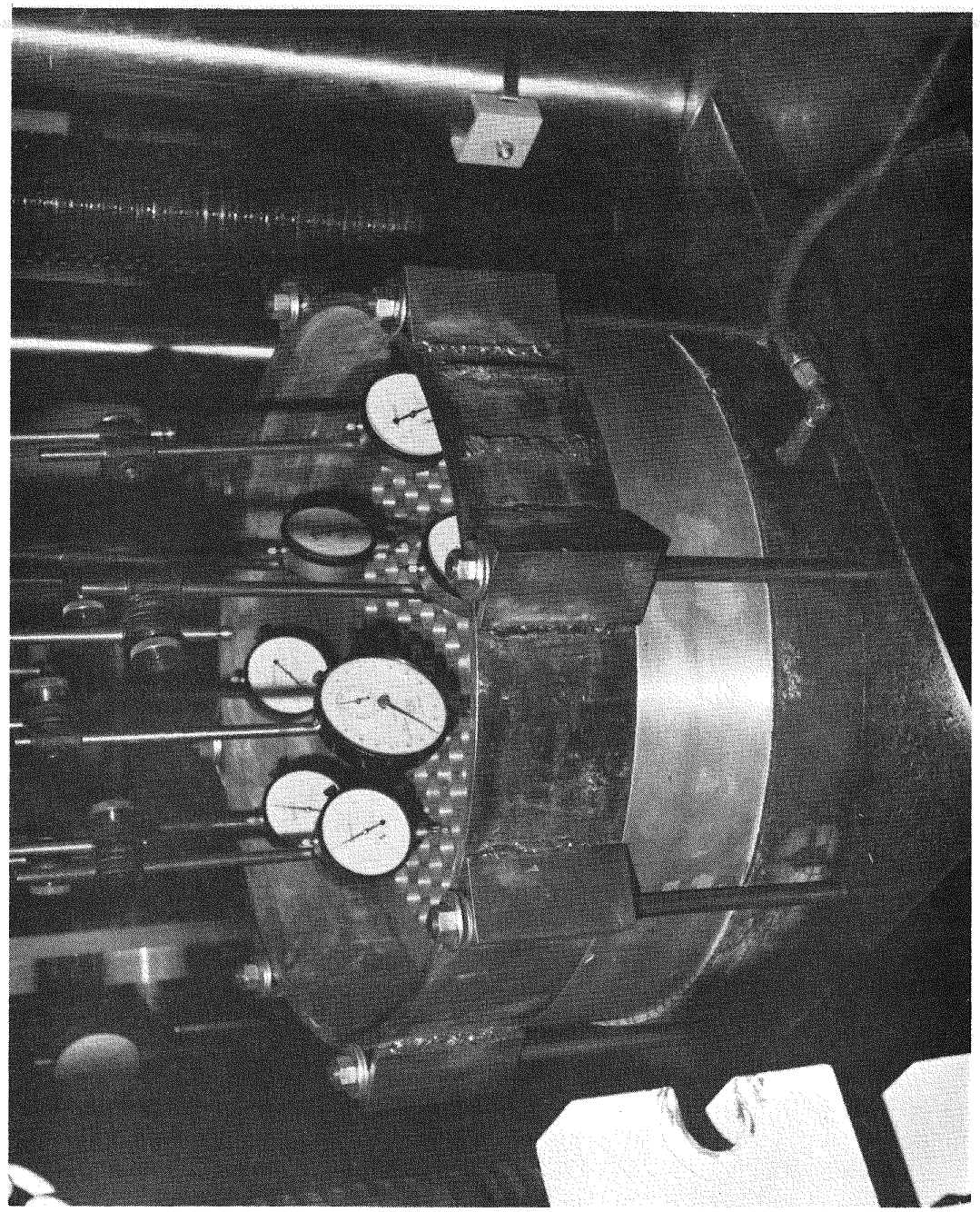

Fig. 5. Axial deflection testing arrangement

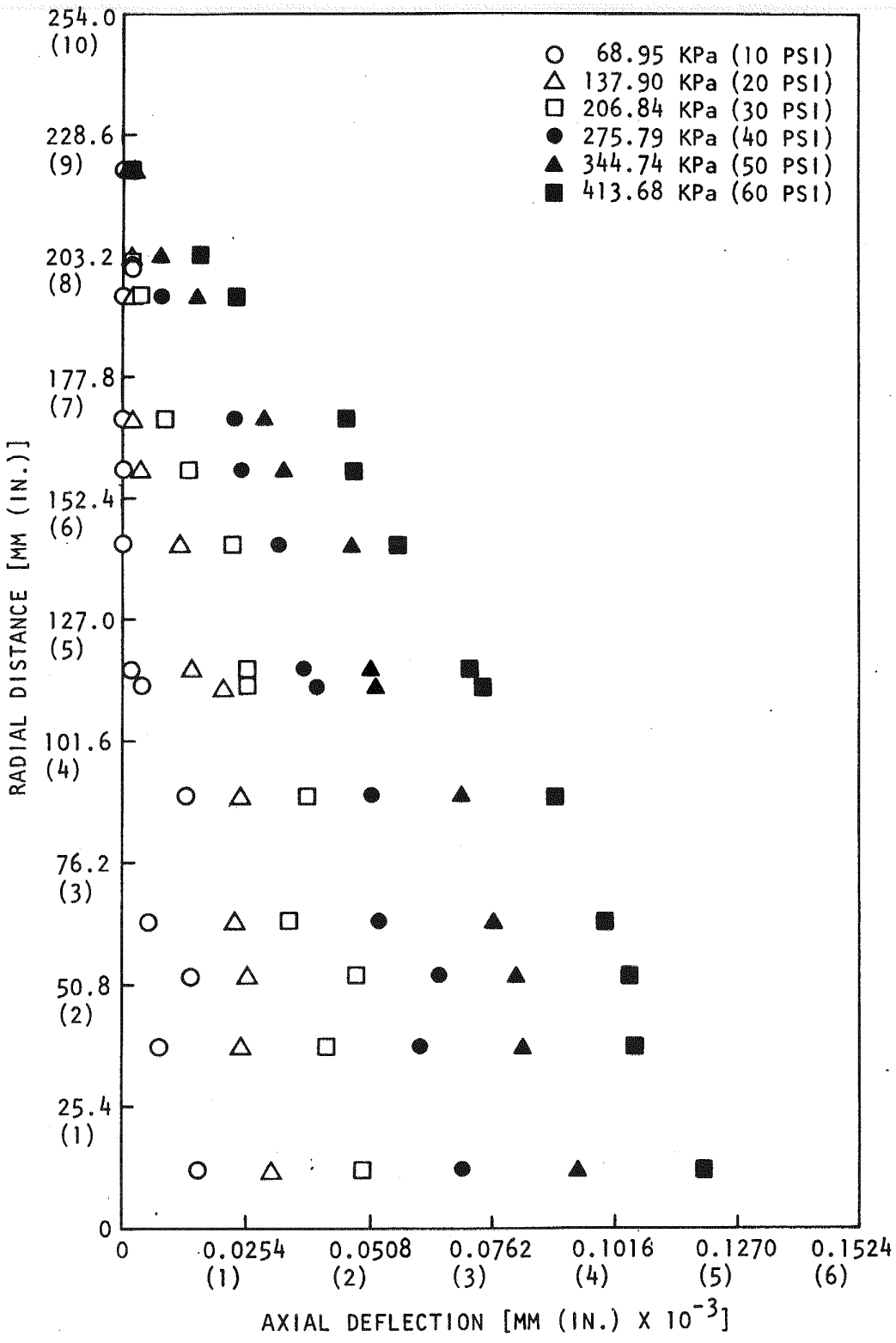

Fig. 6. Axial deflection vs radial distance of grid plate, test results

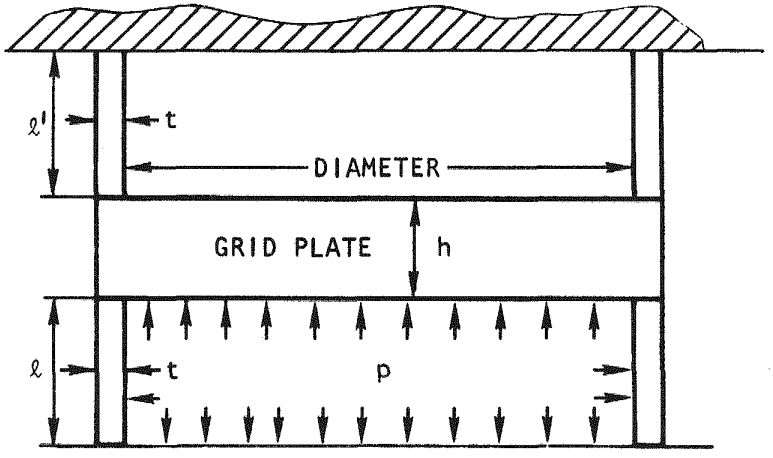

Fig. 7. Schematic test setup

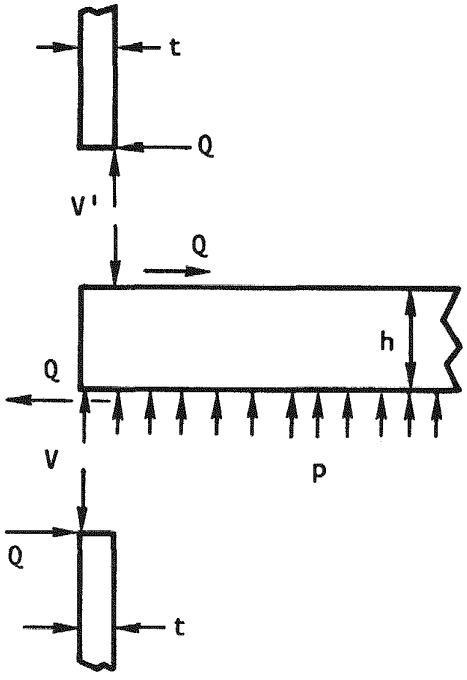

Fig. 8. Free-body diagram of the test grid plate and the support rings

when the grid plate is subjected to a pressure loading. The rotation at the edge of the grid plate can be shown as

$$\theta = \frac{3(1 - \nu^*)pR^3}{2E^*H^3} - \frac{12(1 - \nu^*)R}{E^*H^3}(QH + tV) \quad . \tag{8}$$

The lower support ring can be treated as a short cylinder* subjected to an edge force Q at the upper end and free at the lower end. From Ref. 10, the exact formulas for a short cylindrical shell of uniform thickness subjected to an edge force is

$$u_r = -\frac{Q}{2Dk^3}\left[\frac{F_4}{F_1}F_7(\xi) - \frac{F_5}{F_1}(\xi) - \frac{F_6}{F_1}F_{16}(\xi)\right] \quad , \tag{9}$$

where $k = \frac{\sqrt[4]{3(1 - \nu^2)}}{\sqrt{Rt}}$, and $\xi = \frac{x}{l}$.

F_i and $F_i(\xi)$ are the factors dependent on the type of boundary and loading conditions. They can be expressed in terms of trigonometry and hyperbolic functions.

Using the geometric relationship between u_r and the rotation of the grid plate and the support ring and the compatibility condition between the support ring and the grid plate, the following relation can be derived:

$$(1.6387 \times 10^{-5}\ m^3)\frac{2}{\sqrt{h^2 + t^2}}\frac{2Q}{D} = \frac{3(1 - \nu^*)pR^3}{2E^*h^3} - \frac{12(1 - \nu^*)R}{E^*h^3}(Qh + tV) \quad , \tag{10}$$

where $(1.6387 \times 10^5\ m^3)$ is a conversion factor for SI units.

The shear force V can be expressed in terms of the bolt preload $\bar{p}$ and the pressure load p on the grid plate test model:

$$V = \frac{\bar{p} - \pi(R)^2 p}{2\pi(R)} \quad ,$$

where $\bar{p} = 2.135 \times 10^5$ N (48,000 lb), $p = 413.68$ kPa (60 psi)

$R = 244.475$ mm (9.625 in.).

Thus, $V = 8.8422 \times 10^4$ N/m (504.903 lb/in.). Substituting the numerical values of all the parameters and the values of V and p into eq. (10) yields

$$Q = 1.4349 \times 10^4 \text{ N/m } (81.93 \text{ lb/in.}) \quad .$$

*For a cylinder with $L < 3.1\sqrt{Rt}$

4.3. EFFECT OF CLAMPING ON THE CENTER DEFLECTION OF THE GRID PLATE

The terms w_1 and w_2 are defined as

w_1 = axial deflection at the center of the grid plate due to pressure loading p,
w_2 = reduction of axial deflection at the center of the grid plate due to clamping effect.

In mathematical form, w_1 and w_2 can be written as

$$w_1 = \frac{p}{64D} \frac{5 + \nu^*}{1 + \nu^*} R^4 \quad ,$$

$$w_2 = \frac{6(1 - \nu^*)R^2}{E^* h^3} (Qh + tV) \quad .$$

Substituting all the constants and parameters for w_1 and w_2 and determining the ratio of w_2/w_1 yields $w_2/w_1 = 0.4834$. That is, the clamping effect reduces the center axial deflection of the grid plate model by 48.34%.

5. CONCLUSIONS

Using the analytical approach, the axial deflection at the center of the grid plate due to a 413.68-kPa (60-psi) uniform pressure loading is 0.2384 mm (9.387×10^{-3} in.); the finite-element model gives an axial deflection of 0.2337 mm (9.2×10^{-3} in.). These two results are considered to be in good agreement. However, the test measurement shows that the center deflection of the grid plate model is only 0.1194 mm (4.7×10^{-3} in.). As indicated in Section 4.3, the effect of clamping on the center deflection of the grid plate is 48.34% of the total deflection; therefore, the center deflection of the grid plate should be on the order of 0.1194 mm (4.7×10^{-3} in.) + 0.2384 mm (9.387×10^{-3} in.) (48.34%) = 0.2346 mm (9.238×10^{-3} in.). Comparison of the adjusted testing result δ_{center} = 0.2346 mm (9.238×10^{-3} in.) with the analytical or finite-element result indicates a discrepancy of less than 2% among the three models.

For the case of a point 50.8 mm (2 in.) off the center, under a pressure load of 413.68 kPa (60 psi), the axial deflections obtained by the analytical, testing, and finite-element methods are

1. Analytical: w_a = 0.2235 mm (8.799×10^{-3} in.).

2. Testing: w_t = 0.1067 mm (4.2×10^{-3} in.) + 48.34% x 0.2235 mm (8.799×10^{-3} in.)
   = 0.2147 mm (8.453×10^{-3} in.).

3. Finite-element: w_f = 0.2172 mm (8.55×10^{-3} in.).

There is a 3.9% difference between the analytical and testing results and a 2.8% difference between the analytical and finite-element results. For the case where r = 101.6 mm (4 in.) and p = 413.68 kPa (60 psi),

1. Analytical: $w_a = 0.1812$ mm (7.134×10^{-3} in.).

2. Testing: $w_t = 0.0826$ mm (3.25×10^{-3} in.) + 48.34% x 0.1812 mm (7.134×10^{-3} in.)
   $= 0.1702$ mm (6.699×10^{-3} in.).

3. Finite-element: $w_f = 0.1746$ mm (6.874×10^{-3} in.).

There is a 6.1% difference between the analytical and testing results and a 3.64% difference between the analytical and finite-element results. For the case of r = 152.4 mm (6 in.) and p = 413.68 kPa (60 psi),

1. Analytical: $w_a = 0.1190$ mm (4.685×10^{-3} in.).

2. Testing: $w_t = 0.0546$ mm (2.15×10^{-3} in.) + 48.34% x 0.1190 mm (4.685×10^{-3} in.)
   $= 0.1121$ mm (4.415×10^{-3} in.).

3. Finite-element: $w_f = 0.1135$ mm (4.467×10^{-3} in.).

There is a 5.76% difference between the analytical and testing results and a 4.75% difference between the analytical and finite-element results.

The three models are in good agreement, and the maximum discrepancy between them is about 6%. Because the clamping force induced by the preloaded bolts is not uniformly distributed along the edge of the grid plate, the testing results near the edge of the grid plate model are not accurate enough for comparative purposes. This is the reason that the comparisons were made only up to 152.4 mm (r = 6 in.) The close agreement of the three models not only proves that the analytical derivation and finite-element model are correct, but also indicates that the equivalent Young's modulus E^* and equivalent Poisson's ratio ν^* obtained from Refs. 5 and 6 are accurate.

ACKNOWLEDGMENTS

This work was performed under U.S. Energy Research and Development Administration Contract EY-76-C-03-0167, Project Agreement 23. The testing was conducted by Prof. R. Bedore, Dr. R. D. McGhie, and Dr. S. Dharmarajan of the Department of Aerospace Engineering, San Diego State University, San Diego, California.

REFERENCES

[1] GARDNER, K. A., "Heat-Exchanger Tube-Sheet Design," J. Appl. Mech. 15, 377-385 (1948).

[2] GARDNER, K. A., "Heat-Exchanger Tube-Sheet Design - 2: Fixed Tube Sheets," J. Appl. Mech. 19, 159-166 (1952).

[3] GARDNER, K. A., "Heat-Exchanger Tube-Sheet Design - 3: U-Tube and Bayonet Tube Sheets," J. Appl. Mech. 27 , 25-33 (1960).

[4] LEKNITSKII, S. G., Theory of Elasticity of an Anisotropic Elastic Body," Holden-Day, San Francisco, 1963.

[5] "ASME Boiler and Pressure Vessel Code," Section III, Article A-8000 (ASME 111/2).

[6] SLOT, T., "Stress Analysis of Thick Perforated Plates," Ph.D. Thesis, University of Technology Delft, the Netherlands, September 1972.

[7] LOVE, A. E. H., A Treatise on the Mathematical Theory of Elasticity, 4th Ed., Dover, New York, 1974.

[8] CHANG, K. H., CHUANG, A. S., WASHINGTON, C. E., "A Structural Analysis of the Gas-Cooled Fast Breeder Reactor Core Support," General Atomic, to be published.

[9] BATHE, K. J., WILSON, E. L., PETERSON, F. E., "SAPIV, A Structural Analysis Program for Static and Dynamic Response of Linear Systems," University of California, Berkeley, 1973.

[10] BAKER, E. H., KOVALEVSKY, L., RISH, F. L., Structural Analysis of Shells, McGraw-Hill, New York, 1972.